## References


[1] Bollermann, B., "A Study of 30 km to 200 km Meteorological Rocket Sounding Systems," *Literature and Data Review*, CR-1529, Vol. 1, Pts. 1 and 2, May 1970, NASA.

[2] Graham, J. J., "Ballute Development for Loki-Dart and Arcas Rocketsondes," AFCRL-68-0622, Nov. 1968, Air Force Cambridge Research Labs.

[3] Niederer, P. G., "Development of a High-Altitude Decelerator," CR-66755, Jan. 1969, NASA.

[4] Niederer, P. G., "Development of an Extremely Lightweight High-Altitude Decelerator," *Journal of Spacecraft and Rockets*, Vol. 6, No. 11, Nov. 11, 1969, pp. 1274–1278.

[5] Niederer, P. G. and Lewis, W. F., "Development of a High-Altitude Decelerator: Review and Evaluation of some Lightweight Knitted Canopy Meshes," Rept. ARC-R-362, Jan. 1970, Astro Research Corp., Santa Barbara, Calif.

[6] Niederer, P. G., Lewis, W. F. and Adams, L.R., "Development of a Stokes-Flow Decelerator for High-Altitude Meteorological Rocket Applications," Final Rept. on Contract NAS1-9881, Rept. ARC-R-513, Nov. 1971, Astro Research Corp., Santa Barbara, Calif.

[7] Topping, A. D., "Buckling Resistance of Inflated Cylinders in Bending," Rept. GER-13015, March 1967, Aerospace Corp., Santa Barbara, Calif.

[8] Crawford, R. F., "Strength and Efficiency of Deployable Booms for Space Applications," AIAA Paper 71-396, Anaheim, Calif, 1971.


MAY 1972 J. SPACECRAFT VOL. 9, NO. 5

# Crippling and Buckling of Corrugated Ring-Stiffened Cylinders


DAVID BUSHNELL*

*Lockheed Palo Alto Research Laboratory, Palo Alto, Calif.*



**A finite-difference energy method is used for prediction of crippling, local buckling, and general instability. Reasonably good agreement is obtained between test and theory for shells which cripple due to pure axial compression, shells which cripple due to axial compression combined with hoop compression induced by local radial restraint at rings and boundaries, shells which buckle locally due to axial load path eccentricity, and shells which buckle between ring stiffeners. Crippling loads are calculated by treatment of a portion of the corrugation-sheet combination as a shell of revolution with radius very large compared to a typical dimension of the corrugation. Critical loads for buckling between rings are rather strongly dependent on boundary conditions load eccentricity, and length of cylinder, even for cylinders with many bays.**


## Introduction

THE purpose of this paper is to present the results of some analytical studies of axially compressed, semisandwich, corrugated cylinders representative of payload shrouds for various space systems applications. Ring-stiffened cylinders are analyzed for stress and stability through use of the BOSOR3 computer program.[1] Comparisons are made between test and theory and between various analyses. Effects of ring stiffeners, eccentric loading, boundary conditions, torsional stiffness, and combined mechanical and thermal loading are explored.

The analysis applies to semisandwich, corrugated flat panels and cylindrical shells reinforced by internal z-section rings. The corrugation geometry is given in Fig. 1a, and the ring stiffener geometry in Fig. 1b. In the BOSOR3 analysis, the corrugation is assumed to be bonded to the skin over the entire length $d$ and the rings are treated as discrete structures. The aluminum shell and rings remain elastic.

Figures 2–5 show various types of buckling in corrugated panels and cylinders. Figure 2 shows part of a 12-in.-long and 9.75-in.-wide panel crippled by an axial load/length of

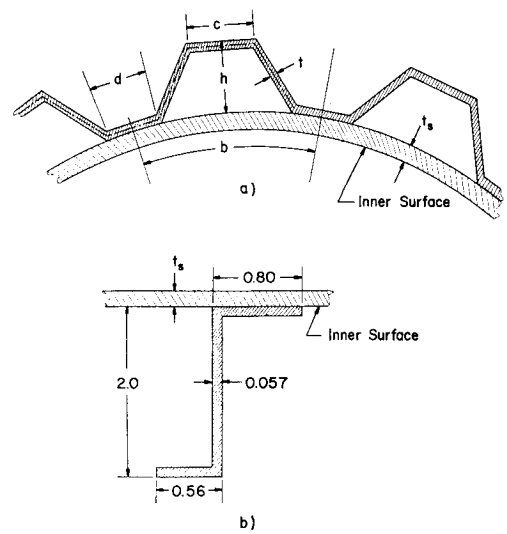


**Fig. 1 a) Semisandwich corrugated wall geometry, and b) Internal discrete ring geometry.**

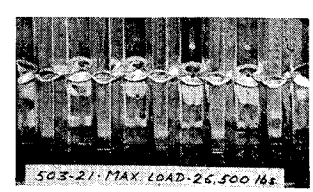


**Fig. 2 Part of 9.75 in. × 12 in. panel with $t$ = 0.020 in., $t_s$ = 0.032 in. crippled under axial compression.**

Received June 1, 1971; presented as Paper 72-138 at the AIAA 11th Aerospace Sciences Meeting, New York, January 17–19, 1972; revision received January 20, 1972. This work is sponsored by the Lockheed Independent Research and Independent Development Programs. The author is grateful for the many fruitful discussions with P. Stern, B. Burns, D. Tenerelli and B. Almroth during the course of this work.

* Staff Scientist. Associate Fellow AIAA.

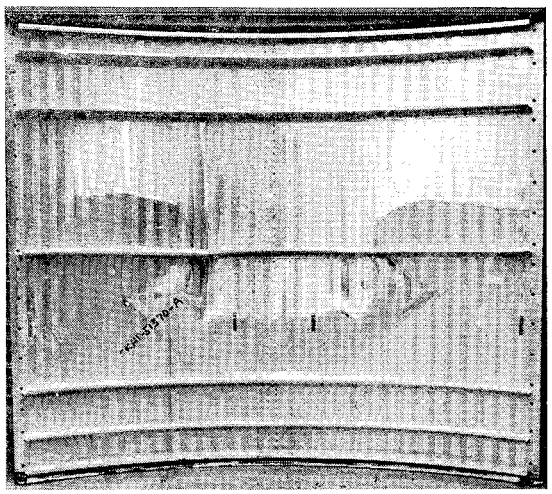

Fig. 3 60 in. × 52 in. curved (60 in. radius) ring-stiffened panel with $t = 0.025$ in., $t_s = 0.040$ in. buckled in general instability mode under uniform axial compression.

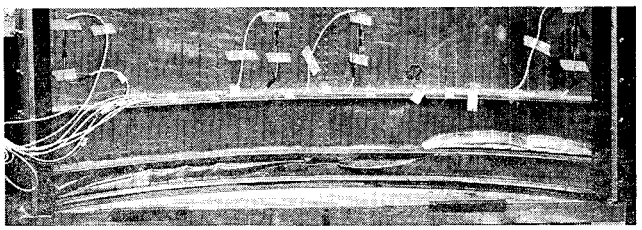

Fig. 4 Part of 60 in. × 52 in. panel and $t = 0.020$ in., $t_s = 0.032$ in. crippled near bottom under uniform axial compression.

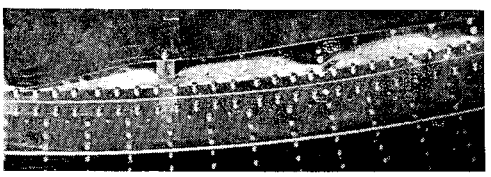

Fig. 5 Interior view of portion of complete cylindrical shroud buckled locally next to a field joint; three waves are visible.

2720. Figure 3 shows a 52-in.-long and 60-in.-wide curved ring-stiffened (60-in.-radius) panel buckled in a "general instability" mode by an axial load of 2550 lb/in. Figure 4 shows part of another ring-stiffened 52 in. × 60 in. panel made of the same gage material as the small panel shown in Fig. 2. This panel crippled locally at the bottom at a load of 1620 lb/in., far below the crippling "allowable" indicated by the small panel test. Figure 5 shows a portion of a buckled cylinder in which buckling under axial compression was very local in the neighborhood of a field joint.

One of the objectives of this paper is to demonstrate that these types of buckling can be predicted analytically. The other objective is to perform parameter studies in order to enhance the understanding of the behavior of semisandwich, corrugated shell structures with regard to stress and stability.

## Analysis Method and Numerical Results

The analysis method on which the BOSOR3 computer program is based is described in detail in Ref. 2. Formulas from which the constitutive equation coefficients for semisandwich corrugated shells are derived are given in Ref. 3.

Stresses and buckling loads were obtained by means of the BOSOR3 computer program for corrugation-skin combinations with dimensions (Fig. 1a) in inches: $b = 1.848$, $h = 0.6$, $c = 0.43$, $t = 0.02$ and 0.025, $d = 0.778$, and $t_s = 0.032$ and 0.040. Thickness combinations $t/t_s$ are referred to in the tables, figures, and text as 020/032 or 025/040. This section is divided into two subsections: analytical correlation with test results and parameter studies.

### Analytical Correlation with Test Results

Table 1 contains a summary of test results with analytical predictions for small flat and large curved panels such as shown in Figs. 2–4 and for a complete cylinder, the buckled portion of which is shown in Fig. 5. Cases 1–10 were tested by Tenerelli and Holmes in the Structural Mechanics Lab., Lockheed Missiles and Space Co., Palo Alto, Calif. Panel manufacturing techniques and test methods are described in detail in Ref. 4. The test in case 11 is fully documented by Bauman in Ref. 5. All curved panels and the complete shroud had radii of 60 in. Table 1 is divided into three sections applicable respectively to small flat panels, large ring-stiffened curved panels, and a complete cylindrical shroud.

*Small panels*

Crippling of the skin and corrugations are analyzed by treatment of a small section of a panel as a shell of revolution. As explained in Ref. 6, this technique can be used for the analysis of prismatic structures: the axial coordinate (direction parallel to the corrugations) becomes the circumferential coordinate of the shell of revolution. Details of deformations around the perimeter of a single corrugation are calculated by use of finite-differences in that direction, and axial variation is assumed to be harmonic. This technique is applicable to simply-supported prismatic shells or to prismatic shells which are long compared to a typical cross-sectional dimension. Figure 6 shows the model. The three-segment shell of revolution consists of two annuli and a conical frustrum. The radius to the axis of revolution is chosen very large compared to a typical segment length. Axial wavelengths of the buckle pattern are inversely proportional to the circumferential wavenumber $n$. The branch corresponding to the section where corrugation and skin are welded together is ignored. The three-segment meridian is presumed to be uniformly compressed in the hoop direction, that is in the direction normal to the plane of the paper. Critical stresses

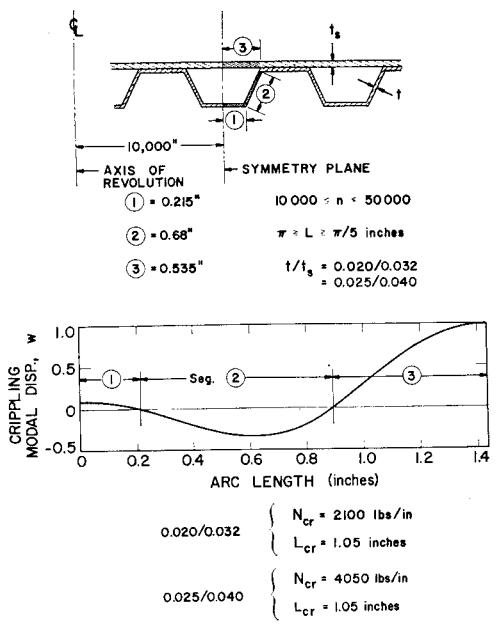


Fig. 6 Portion of aluminum corrugated shell wall treated as shell of revolution with 10,000 in. radius.

are calculated for $10{,}000 \leq n \leq 50{,}000$. The minimum critical stress corresponds to $n = 30{,}000$ or an axial half-wavelength of 1.05 in., about the same as twice the length of segment 3. The normal displacement component $w$ of the buckling mode is shown, and the critical equivalent loads/length for 020/032 and 025/040 gage combinations are given. The test panels buckled somewhat above these predicted loads, presumably because structures consisting essentially of an assemblage of flat plates can carry axial loads in excess of their bifurcation buckling loads.

*Large curved panels*

Cases 5–8 in Table 1 apply to ring-stiffened panels of the type shown in Fig. 3. Cases 9 and 10 represent panels of geometry similar to that shown in Fig. 3, except that there are six bays of 16-in. length instead of two. The heavily reinforced cutout referred to in case 10 was located in the middle two 16-in. bays. All curved panels were analyzed as if they were complete cylindrical shells.

Figure 7 gives comparisons between test and theory for

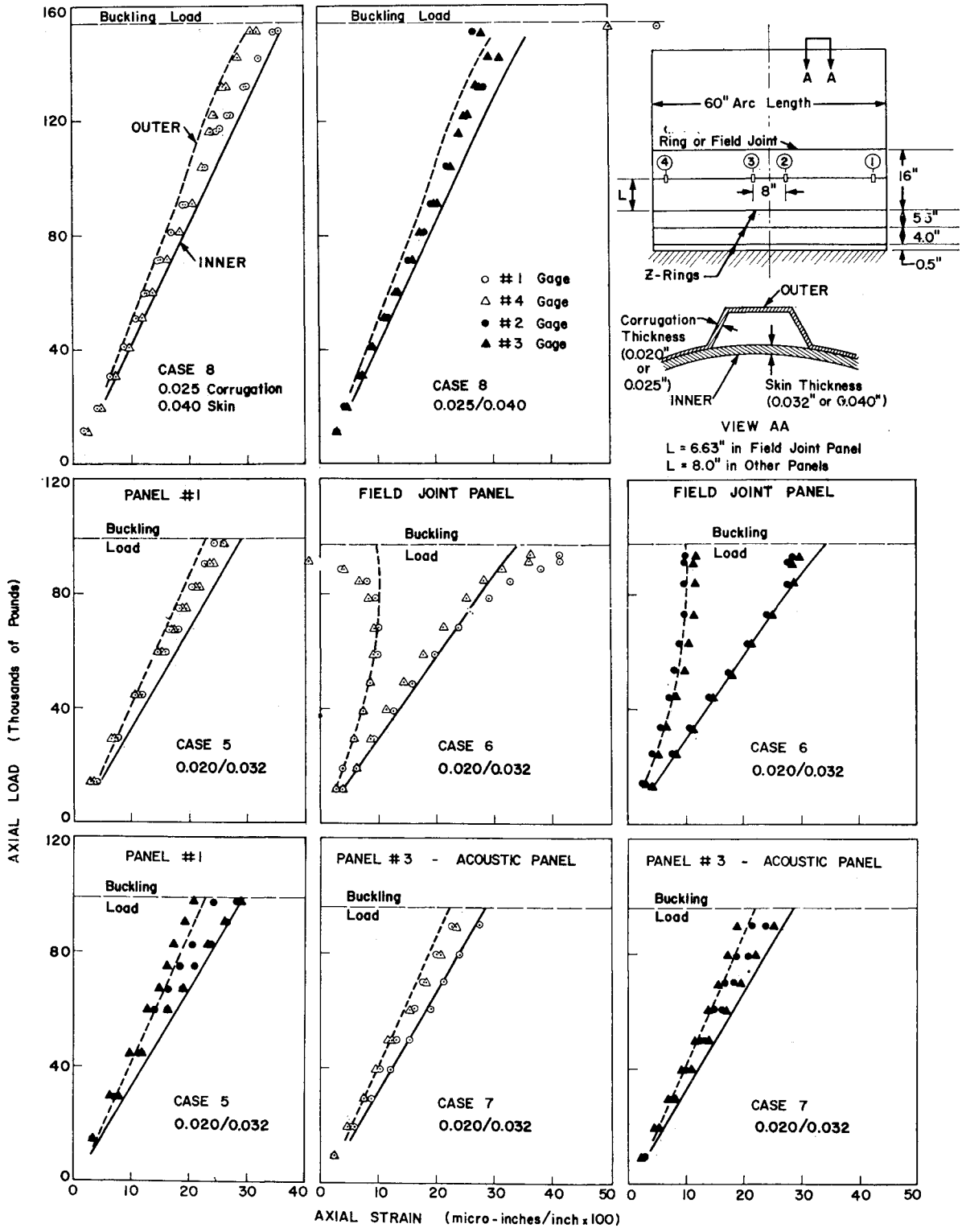


**Fig. 7 Comparison between test and theory for prebuckling strains in 60 in. × 52 in. curved panels, Cases 5–8 in Table 1.**

**Table 1 Comparison of test and theory for critical axial loads on corrugated panels**

| Case | Type of specimen | Test load lb/in. | Observed buckling mode | Analytical predictions lb/in. | | Comments |
|---|---|---|---|---|---|---|
| | | | | Crippling | General instability | |
| 1 | 9.75 in. × 12 in. panel 020/032 | 2930 | Crippling | 2100 | | Panel exhibits post-buckling strength |
| 2 | Same as 1 | 2720 | Crippling | 2100 | | Same as above |
| 3 | 10 in. × 12 in. panel 025/040 | 4250 | Crippling | 4050 | | Panel buckles in plastic region |
| 4 | Same as 3 | 4310 | Crippling | 4050 | | Same as above |
| 5 | 52 in. × 60 in. curved panel, #1: 020/032 | 1640 | Crippling in middle of large bay | 1620 | 2287(13)[a] | Buckling mode not predicted by theory |
| 6 | 52 in. × 60 in. curved panel, #2: 020/032 with field joint | 1620 | Crippling at bottom edge | 1620 | 3450(0) | Forced crippling due to hoop compression at edge, see Fig. 4 |
| 7 | 52 in. × 60 in. curved panel, #3: 020/032 | 1600 | Crippling near ring at top | 1620 | 2287(13) | Buckling mode not predicted by theory |
| 8 | 52 in. × 60 in. curved panel: 025/040 | 2550 | General instability | 3200 | 2800(13) | See Fig. 3 |
| 9 | 116 in. × 60 in. curved panel: 020/032 | 1580 | General instability | 1620 | 1680(16) | |
| 10 | 116 in. × 60 in. curved panel with heavily reinforced cutout | 1650 | Crippling at bottom edge | 1620 | | Forced crippling due to hoop compression at edge |
| 11 | Full shroud with combined shear and axial compression | 1280[b] | Local buckling at field joint | 1520(35)[c] | | Buckling due to eccentric load path near joint, see Fig. 5 |

[a] Numbers in parenthesis are circumferential wavenumbers.
[b] Nominal line load from both shear load and axial compression at point of maximum compression.
[c] Buckling neither crippling nor general instability; see Figs. 5 and 10.

prebuckling inner and outer fiber axial strain at four locations on each panel. Results from cases 5–8 are shown. The large difference in behavior between the panel with the field joint and the other panels is explained by the local inward excursion of the load path through the joint and the massive ring there (shown in Fig. 8). Normal displacements for a compression load of 1750 lb/in. for panels with and without field joints are shown in Fig. 8, revealing the comparatively large amount of bending present in the field joint panel.

The plot of computed hoop force at the bottom of Fig. 8 is included to emphasize the fact that the clamped boundary and ring stiffeners prevent radial expansion due to the Poisson effect, thus causing the skin to be circumferentially compressed. This compression serves to lower the crippling load considerably, as will be shown presently.

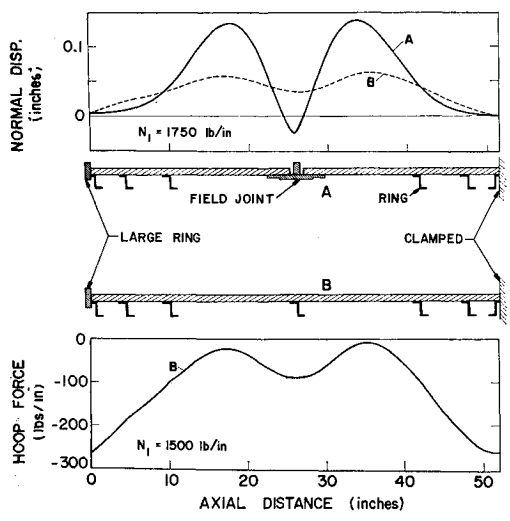


**Fig. 8 Theoretical prebuckling behavior of 60 in. × 52 in. curved panels with and without field joint.**

Table 1 gives two theoretical buckling loads for Cases 5–9, crippling and general instability. The general instability loads are calculated with torsional stiffness factor $\phi = 0.3$ (see Ref. 3) and approximately 100 mesh points. Figure 9 shows the predicted general instability buckling mode shape for Cases 5 and 7. The mode shape for Case 8 is almost identical. The $z$-rings are of such a size in all cases that buckling occurs between them, that is the normal modal displacements at the ring attachment points are small compared to those between rings. Hence, the column heading "General Instability" in Table 1 may be somewhat misleading. However, the mode shape shown in Fig. 9 corresponds to the smallest eigenvalue of a stability matrix calculated in such a way that a true general instability mode (rings undergoing considerable normal displacement) is permitted by the analysis. In this sense and in the sense that the buckle pattern spans several corrugations in the circumferential direction, the calculated eigenvalues represent "general instability" buckling loads.

The crippling loads are calculated with the same mathematical model (Fig. 6) as that used for the small flat panels,

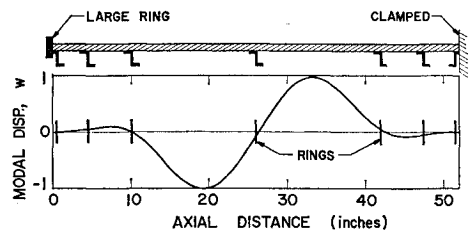


**Fig. 9 Theoretical buckling modal displacement for "general instability" in Cases 5, 7 and 8 in Table 1.**

except that the presence of axial bending and skin hoop compression is accounted for. The procedure for calculating these "forced" crippling loads is as follows: the stress distribution over the corrugation cross section as a function of axial distance is determined for a given axial load. A particular axial station is then chosen as the most likely site of initial crippling. The stress distribution in the three segments labeled 1, 2, and 3 in Fig. 6 is then used in the type of stability analysis discussed with regard to the small flat panels. For example, in Cases 5–10, it was determined that the "worst" axial station corresponds to the clamped edge at the bottom of the panels where the hoop stress resultant in Fig. 8 is maximum negative. At this station for the 020/032 panels loaded to 1500 lb/in. compression the axial stress $\sigma_1$ in the outer crown of the corrugation is $-36$ kips, in the skin it is $-24$ kips, and it varies linearly between. The hoop stress in the skin is $-8.1$ kips. With this prestress distribution, the predicted bifurcation buckling axial load/length is 1620 lb/in. A similar procedure leads to a prediction of forced crippling at 3200 lb/in. for the 025/040 panel. The forced crippling mode shapes resemble that in Fig. 6.

Note that comments "Buckling mode not predicted by theory" are entered in Table 1 opposite Cases 5 and 7. This is because the crippling occurred at sites other than that associated with the maximum compressive hoop stress. Also note that while the crippling load predictions for the small panels are somewhat below the test loads, indicating postbuckling strength, the forced crippling load predictions for the large curved panels are very close to the failure loads, indicating no postbuckling strength.

*Cylinder with failure at field joint*

A full-scale cylindrical shroud was tested under combined shear and axial compression. This test is listed as Case 11 in Table 1. The shear load was applied by means of a belly band that spanned many rings. The axial load was applied by means of a cable along the cylinder axis pulled from the bottom. Axial load and shear were increased in proportion until at a combined (axial, shear) load of 34700, 36600 lbs, failure occurred locally on the side of maximum compression at a field joint. Figure 5 shows the local buckling failure. The maximum nominal axial load at the field joint was 1280 lb/in. It is felt that the actual maximum line load was perhaps 10–20% higher than this due to local stress concentrations at the ends of big longerons not shown in Fig. 5.

In the BOSOR3 model of the shroud, the loading was assumed to be axisymmetric axial compression. Figure 10a shows the normal displacement corresponding to 1 lb/in. compression. As the axial load is increased, large hoop compressive stresses build up in the segment just forward of the large field joint ring. These stresses combined with the axial compression cause buckling as shown in Fig. 10b at a predicted axial load of 1520 lb/in. corresponding to 35 circumferential waves. Behavior prior to buckling is rather nonlinear in the neighborhood of the field joint.

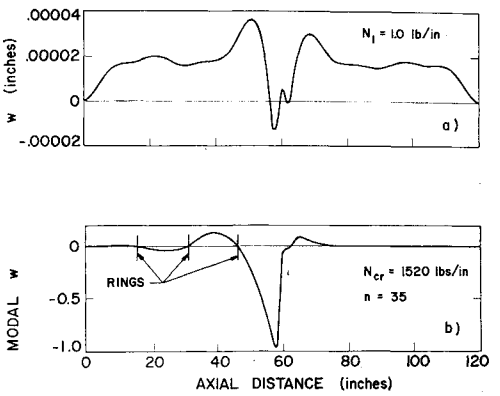


**Fig. 10 Prebuckling and buckling behavior of 60 in.-radius, ring-stiffened cylinder with field joint: a) normal outward axisymmetric displacement with axial compression of 1.0 lb/in., and b) buckling modal displacement.**

## Parameter Studies

Four studies are documented in this section: analysis of 60-in.-radius, 15-in.-long corrugated cylinders with various boundary conditions, torsion factors $\phi$, and load eccentricities; analysis of 60-in.-radius, ring-stiffened corrugated cylinders of various lengths; a forced crippling analysis with various combinations of axial and hoop stress; and a stress analysis of a ring-stiffened, corrugated cylinder under combined axial compression and nonsymmetric heating. All studies are performed for corrugation-skin combinations with dimensions (Fig. 1a): $b = 1.848$, $h = 0.6$, $c = 0.43$, $t = 0.02$, $d = 0.778$, and $t_s = 0.032$.

### Corrugated Cylinder Bay

Table 2 gives critical axial compressive loads for 60-in.-radius, 15-in.-long corrugated cylinders with various boundary conditions, torsion factors $\phi$ and load eccentricities $z^*$. Comparisons are made between the cylinders treated as corrugated and as eccentrically stiffened.

Several interesting facts emerge from an inspection of Table 2. 1) The predicted buckling loads for simply supported shells depend rather strongly on the load eccentricity $z^*$, especially for small values of torsion factor $\phi$. This dependence arises from the prebuckling hoop forces induced in the shell because of the load eccentricity. Induced hoop tension which results from axial loading inside the neutral axis

**Table 2 General instability critical axial loads/length (lb/in.)[a]**

| Boundary conditions | Torsion factor $\phi$[c] | As corrugated | | As stiffened | |
|---|---|---|---|---|---|
| | | $z^{*d} = 0.016$ | $z^* = 0.118$ | $z^* = 0.016$ | $z^* = 0.118$ |
| Simple support | 0.0 | 1800(13)[b] | 1090(30) | 2365(10) | 1493(43) |
| Simple support | 0.2 | | 1427(20) | | |
| Simple support | 0.3 | | 1533(16) | | |
| Simple support | 0.4 | | 1623(16) | | |
| Simple support | 1.0 | 2352(9) | 2030(13) | 2658(7) | 2440(9) |
| Clamped | 0.0 | 2799(32) | | | |
| Clamped | 1.0 | 4869(20) | | | |

[a] For 60-in.-radius, 15-in.-length, semisandwich corrugated cylinders with $t/t_s = 0.020/0.032$.
[b] Circumferential wavenumbers given in parentheses.
[c] See Ref. 3.
[d] Distance from shell inner surface to reference surface.

(small values of $z^*$) raises the buckling load, just as internal pressure would. Induced hoop compression, of course, has the opposite effect. It was primarily this induced hoop force which caused the buckling failure of the field joint shown in Fig. 5. 2) The predicted buckling loads depend strongly on the torsion factor $\phi$. The sensitivity to $\phi$ increases as the load eccentricity $z^*$ increases. 3) For this particular cylinder, which is very short compared to the diameter, the critical axial load is very sensitive to boundary conditions. 4) Treatment of corrugated cylinders as eccentrically stiffened shells (neglecting the in-plane shear-carrying capability of the corrugated sheet) results in nonconservative estimates of the buckling loads. This is because the resulting coupling term $C_{36}$ is thus incorrectly calculated. Even though the direct shear term $C_{33}$ is smaller with corrugated sheet shear strength neglected, the over-all effect of the approximation is to increase the predicted buckling loads, since the influence of $C_{36}$ dominates (see Ref. 3 for definitions).

### Corrugated Cylinders with Rings on 15-In. Centers

Figure 11 shows critical loads for clamped cylinders of various lengths with internal $z$-rings of the geometry shown in Fig. 1b on 15-in. centers. The asymptote represents the buckling load of a simply-supported bay 15 in. long and loaded at the shear center $z^* = 0.118$ in. from the inner surface. The buckling wavenumber $n = 16$ in all cases. It is surprising that the boundary conditions significantly affect the buckling load for shells with many bays. Since buckling occurs between rings, as shown by the sketch labeled "Typical Buckle Pattern" one might think that the critical load would approach the asymptote very rapidly as the number of bays is increased.

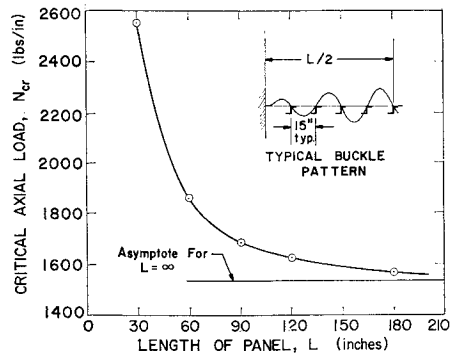


**Fig. 11 Theoretical buckling loads for clamped cylinders of various lengths with discrete rings on 15 in. centers; torsion factor $\phi = 0.3$.**

Figure 12 helps to explain this slow convergence phenomenon. A 200-in.-long corrugated shell without ring stiffeners is loaded by a one in.-lb/in. moment which varies harmonically around the circumference. The nonsymmetric moment simulates the effect of the boundary on the shell during transition from an axisymmetric prestressed state to a nonsymmetric post-buckling state. This study demonstrates the necessity of careful definition of the boundary conditions in tests and analyses of corrugated shells, even if intuition may indicate that they will not affect the buckling behavior.

### Forced Crippling of Biaxially Stressed Corrugated Panels

Figure 13 shows the effect of hoop stresses $\sigma_2$ on the predicted forced crippling load of axially compressed corrugated panels. The results were obtained with the model shown in Fig. 6. The stresses are assumed to be uniformly distributed over the corrugation and face sheet. Predicted crippling loads for Cases 1 and 2 in Table 1 correspond to the minimum point on the curve labeled $\sigma_2/\sigma_1 = 0$. The forced crippling load for Cases 5, 6, 7, 9, and 10 corresponds to a point slightly below the minimum of the curve labeled $\sigma_2/\sigma_1 = 0.25$.

### Temperature Effects

Rapid heating of a corrugated shroud during ascent can introduce additional stresses associated with nonuniform circumferential temperatures and differences in temperature between shell and rings. Figure 14 shows stresses in the skin and in the crown of the corrugation for a ring-stiffened shell of the same geometry as Cases 5–7 in Table 1. The rings are assumed to be at ambient temperature and the shell heated uniformly along the length and nonuniformly around the circumference as shown in the inserted table of $\Delta T$ vs $\theta$. In addition to the thermal input, the shell is subjected to axial compression by a load of 1500 lb/in. The large hoop stresses are caused by restraint imposed on expansion of the shell at "cold" rings and at the clamped boundary. The large outer fiber axial stresses are caused by local axial bending near the center ring and near the clamped boundary. These additional thermal stresses would clearly cause forced crippling at rather small axial loads, and could lead to crippling with no axial load at all. While this case is perhaps a bit extreme, it does illustrate an additional effect which must be accounted for in the design of corrugated payload shrouds.

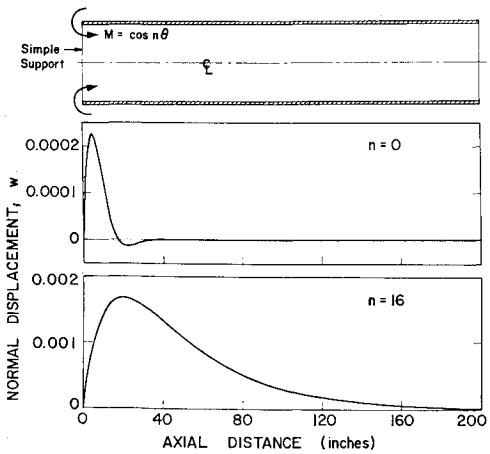


**Fig. 12 Decay of normal displacement for corrugated cylinder with harmonically varying edge moment.**

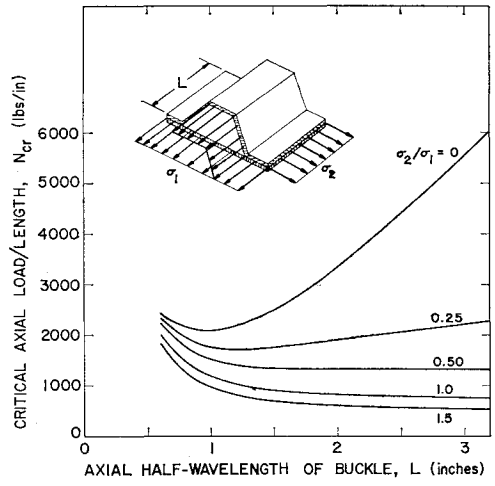


**Fig. 13 Forced crippling loads for biaxially compressed corrugated shell wall.**

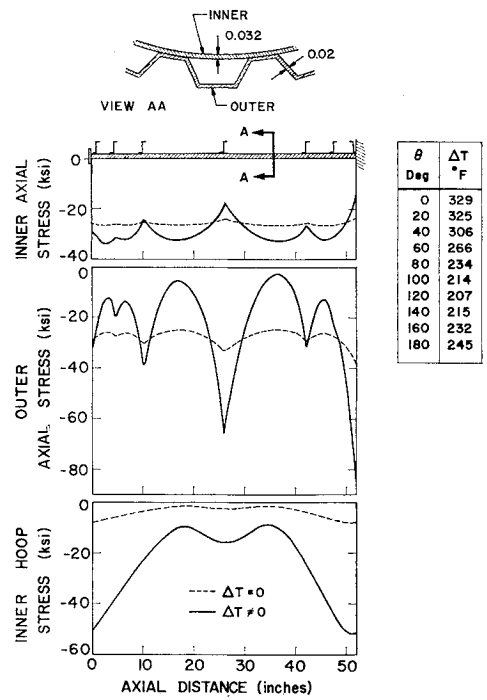


**Fig. 14 Effect of temperature on stress in corrugated panel under 1500 lb/in. compression; discrete rings always at room temperature and shell skin and corrugation heated uniformly through thickness.**

## Conclusions

A finite-difference energy method is used for the stress and buckling analysis of semisandwich externally corrugated cylinders with internal ring stiffeners. Failures due to local crippling under pure axial compression and crippling due to combined axial compression and local hoop compression induced by radial restraint at rings and/or boundaries are predicted by treatment of a portion of the corrugation-sheet combination as a three-segment shell of revolution with radius very large compared to a typical dimension of the corrugation. The presence of hoop compression reduces the predicted axial crippling load significantly. This effect is verified by test results. Local buckling caused by axisymmetric excursions in the axial load path is predicted for corrugated cylinders with field joints of certain configurations. The critical axial load corresponding to buckling between rings depends rather strongly on boundary conditions, length of cylinder, load eccentricity, and details of the mathematical model of the shell wall, that is, certain coefficients $C_{ij}$ of the constitutive equations. In particular, proper estimates of the torsional stiffness $C_{66}$ and the in-plane shear-twist coupling $C_{36}$ are required for reasonably accurate prediction of the behavior.

## References

[1] Bushnell, D., "Stress, Stability, and Vibration of Complex Shells of Revolution: Analysis and User's Manual for BOSOR3," SAMSO TR-69-375, LMSC N-5J-69-1, Sept. 1969, Lockheed Missiles and Space Co., Palo Alto, Calif.

[2] Bushnell, D., "Analysis of Ring-Stiffened Shells of Revolution Under Combined Thermal and Mechanical Loading," *AIAA Journal*, Vol. 9, No. 3, March 1971, pp. 401–410.

[3] Bushnell, D., "Local and General Buckling of Axially Compressed, Semi-Sandwich, Corrugated, Ring-Stiffened Cylinders," AIAA Paper 72-138, San Diego, Calif., 1972.

[4] Tenerelli, D. J. and Holmes, A. M. C., "An Experimental Buckling Study of Skin Corrugated, Ring-Stiffened Curved Panels," SESA Paper 1993A, presented at 1972 meeting of the Society of Experimental Stress Analysis, Cleveland, Ohio, May 23–26, 1972.

[5] Bauman, R. E., "Static Structural Test Evaluation of Shroud," LMSC 62-61/S/R-5, April 1970, Lockheed Missiles and Space Co., Sunnyvale, Calif.

[6] Bushnell, D., "Stress, Buckling and Vibration of Prismatic Shells" *AIAA Journal*, Vol. 9, No. 10, Oct. 1971, pp. 2004–2013.